Frequency Upshift of the Transverse Optical Phonon Resonance in GaAs by Femtosecond Electron-Hole Excitation

Ahmed Ghalgaoui, Klaus Reimann, Michael Woerner,* and Thomas Elsaesser
Max-Born-Institut für Nichtlineare Optik und Kurzzeitspektroskopie, 12489 Berlin, Germany

Christos Flytzanis
Laboratoire de Physique, École Normale Supérieure, Université PSL, 75231 Paris, France

Klaus Biermann
Paul-Drude-Institut für Festkörperelektronik, 10117 Berlin. Germany

(Received 30 October 2019; accepted 22 June 2020; published 10 July 2020)

The impact of transient electric currents on the transverse optical (TO) phonon resonance is studied after excitation by two femtosecond near-infrared pulses via the fourth-order nonlinear terahertz emission. Nonlinear signals due to interband shift currents and heavy-hole–light-hole polarizations are separated from Raman-induced TO phonon coherences. The latter display a frequency upshift by some 100 GHz upon interband excitation of an electron-hole plasma. The frequency shift is caused by transverse electronic shift currents, which modify the dielectric function. A local-field model based on microscopic current densities reproduces the observed frequency upshift.

DOI: 10.1103/PhysRevLett.125.027401

The frequency of lattice vibrations or phonons in crystals is determined by the electronic structure of the periodic solid. The adiabatic approximation for isolated oscillators has frequently been applied to describe phononic properties in the electronic ground state, where the valence electron structure defines the relevant potential energy surface [1]. The picture of isolated oscillators breaks down in polar crystalline materials, where local electric fields modify both the vibrational and dielectric response [2]. Particular molecular vibrations [3] and transverse optical (TO) phonons [4,5] couple to the electronic system. The so-called soft modes at terahertz (THz) frequencies are shifted to higher frequencies upon resonant vibrational excitation, a behavior which is due to a breakup of electronic correlations induced by the vibrational excitation.

In a local-field picture [2,6,7], a vibrational transition dipole experiences the average macroscopic electric field $\mathbf{E}$ in the sample and its own macroscopic polarization contribution $\mathbf{P}$ according to $\mathbf{E}_{\mathrm{loc}} = \mathbf{E} + \mathbf{P}/(3\varepsilon_0)$ (ε_0 is the vacuum permittivity). Both nuclear motions of polar groups and relocations of electronic charge, i.e., time-integrated currents, contribute to the frequency-dependent polarization term, as has recently been shown in ultrafast THz and x-ray experiments on the molecular crystal aspirin [3,8,9]. From a theoretical point of view, the *microscopic* current densities within the unit cell represent the sources of polarization [10,11].

Electronic excitation induces a change of the electronic charge distribution and local electric polarization and, thus, should affect the vibrational properties of the crystal lattice. For polar III–V semiconductors such as GaAs, the coupling of transverse electronic currents and TO phonons should induce a phonon frequency shift via the dielectric function of the coupled system and/or via changes of the vibrational potential. While TO phonon frequencies of GaAs have been studied as a function of external hydrostatic pressure [12,13], the impact of transient electric polarizations and ultrafast electric currents has not been considered. Moreover, it has been neglected in standard treatments of the dielectric function [14]. It is important to note that the coupling considered here is fundamentally different from the interaction of longitudinal optical phonons with plasmons [15,16].

Optical excitation across the fundamental band gap of GaAs is connected with a change of the electronic charge distribution within the unit cell, generating a nonlinear electric shift current [17–20]. This interband current is due to a shift of electronic charge from the covalent bonds between Ga and As atoms onto the Ga sites [Figs. 1(a)–1(c)]. Femtosecond interband excitation of a (111)-oriented GaAs sample generates a short-lived transverse shift current with a time structure following the second derivative of the pulse envelope and giving rise to THz emission [21]. The transverse character of this current allows for exploring its impact on TO phonons.

In this Letter, we demonstrate, for the first time, the impact of transverse electronic currents on TO phonons in bulk GaAs, exploiting a highly sensitive scheme of two-dimensional (2D) spectroscopy. A sequence of two femtosecond near-infrared pulses generates an interband

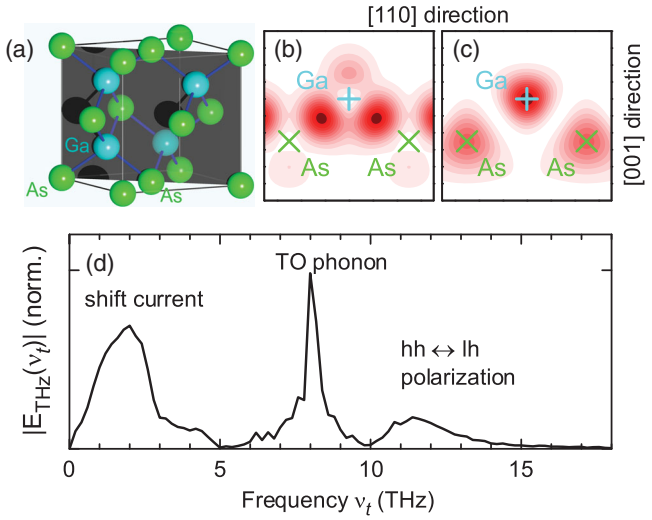

FIG. 1. (a) Unit cell of GaAs. Electronic charge density in the $(1\bar{1}0)$ plane [shaded plane in (a)] for the highest valence band (b) and the lowest conduction band (c). (d) Measured THz spectrum induced by the single near-infrared pulse B, consisting of a shift-current component around 2 THz, a TO-phonon component at 8 THz, and a component emitted by coherent hh ↔ lh inter-valence-band polarizations above 10 THz [21].

excitation and coherent TO phonons. Phase-resolved detection of the THz emission from the excited sample allows for mapping the impact of the electronic current on the TO phonon frequency. We observe a transient frequency upshift by some 100 GHz, which originates from a modification of the dielectric function by the local electric polarization. A theoretical local-field picture reproduces the magnitude of the frequency change.

In our experiments, a pair of phase-locked collinearly propagating near-infrared pulses A and B excites a (111) oriented bulk GaAs sample of 250 nm thickness mounted on a glass substrate [21]. The delay time τ between the two pulses is measured relative to pulse B. For negative delay times ($\tau < 0$), pulse A interacts with the sample before pulse B. Both pulses have a linear polarization along the $[1\bar{1}0]$ direction of the sample. The THz field emitted by the sample with a linear polarization along the $[11\bar{2}]$ direction is detected in a phase-resolved way by electro-optic (EO) sampling with a weak near-infrared sampling pulse. There are two independent time variables in this scheme, the delay time τ between the two excitation pulses and the real time t of the phase-resolved THz detection. The nonlinear THz emission signal is given by $E_{\mathrm{NL}}(t,\tau) = E_{AB}(t,\tau) - E_A(t,\tau) - E_B(t)$, where $\mathrm{E}_{AB}(t,\tau)$ is the THz electric field emitted after interaction with both near-infrared pulses and $E_A(t,\tau)$ and $E_B(t)$ the THz emission after interaction with near-infrared pulses A or B, respectively. A 2D Fourier transform of this differential signal along τ and t generates 2D spectra $|E_{\mathrm{NL}}(\nu_\tau,\nu_t)|$ of the THz emission as a function of the excitation frequency ν_τ and detection frequency ν_t [22,23].

Femtosecond near-infrared pulses were generated at a 1 MHz repetition rate in an optical parametric amplifier (OPA; Opera-F, Light Conversion) pumped by an Yb-based laser system (Monaco, Coherent). The OPA output at a center frequency of $\nu_0 = 350$ THz (850 nm) was compressed to a pulse duration of 25 fs and split into the two excitation pulses A and B and a third component, which serves as the probe pulse in the EO sampling setup. The near-infrared excitation pulses have pulse energies of 0.23 (A) and 0.18 μJ (B). The two Gaussian beams have a diameter of 3 mm on the GaAs sample. From the fluences of pulses A and B and the optical thickness of the GaAs sample, one estimates an excitation density of $1.0 - 3.0 \times 10^{17}$ electron-hole pairs/cm^3, corresponding to less than $2 \times 10^{-4}/a^3$ (a^3: volume of the GaAs unit cell with $a = 0.565$ nm). A 10 μm-thick (110)-oriented ZnTe layer attached to a thick inactive (100)-oriented ZnTe substrate is used for electrooptic sampling with a detection bandwidth of approximately 18 THz. All measurements are performed in a nitrogen atmosphere at ambient temperature ($T = 300$ K).

The nonlinear THz emission of GaAs induced by interaction with the single near-infrared pulse B consists of the three components shown in Fig. 1(d). As has been discussed in detail in Ref. [21], the interband shift current (SC) gives rise to the emission between 0 and 3 THz, the peak around 8 THz is due to coherent TO phonon (TO) excitations, and the component above 10 THz to coherent heavy-hole–light-hole (hh ↔ lh) polarizations. The underlying generation processes are of second order in the electric field of pulse B: The shift current is generated via two resonant interactions with the pump field, promoting electrons from the valence to the conduction band, while the TO phonon and hh ↔ lh polarizations are created via second-order Raman processes within the bandwidth of the near-infrared pulse. They radiate via their (THz active) transition dipole.

The experiments with two near-infrared pulses A and B go beyond the second-order regime and give new insight into the GaAs response at higher nonlinear orders. In Fig. 2(a), the THz field $E_{\mathrm{NL}}(t,\tau)$ generated by interaction of both pulses A and B with the GaAs sample is plotted as a function of the real time t (abscissa) and the delay time τ (ordinate). The corresponding 2D spectrum $|E_{\mathrm{NL}}(\nu_t,\nu_\tau)|$ shown in panel (b) covers a frequency range of $\nu_\tau = \pm 18$ and $\nu_t = \pm 18$ THz [24]. The 2D spectrum displays pronounced peaks at $(\nu_t,\nu_\tau) = (2,0)$, (8,0), (12,0), $(2,-2)$, $(8,-8)$, and $(12,-12)$ THz. Applying a Gaussian 2D frequency filter on the individual spots and performing a 2D Fourier back transform of the peaks at (8,0) and $(8,-8)$ THz, we derive the time dependent 2D signals shown in Figs. 2(c) and 2(d).

The (ν_t,ν_τ) frequency range plotted in Fig. 2(b) is well below the carrier frequency of the near-infrared pulses A and B of 350 THz. The generation of nonlinear THz signals

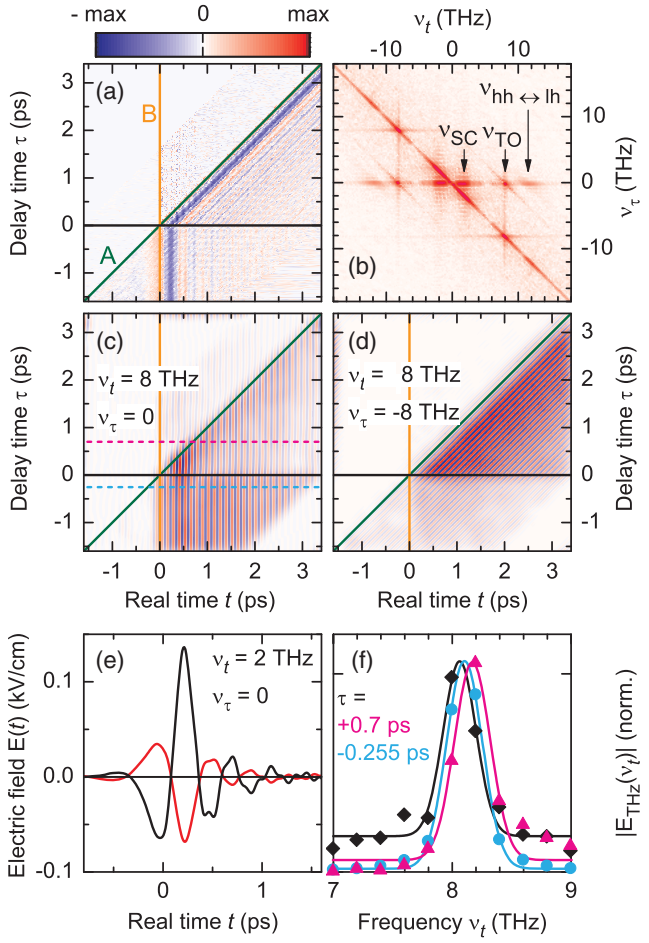

FIG. 2. (a) Contour plot of the nonlinearly emitted electric field $E_{NL}(t,\tau)$ as a function of real time t and delay time τ. (b) Contour plot of the 2D Fourier transform of the measured nonlinear signal in panel (a) as a function of the excitation frequency ν_τ and the detection frequency ν_t. Frequency positions of the shift current (SC), TO phonons, and hh ↔ lh intervalence-band polarizations are indicated by arrows. Fourier back transforms of the TO-phonon signals at $(\nu_t,\nu_\tau) = (8,0)$ THz (c) and at $(\nu_t,\nu_\tau) = (8,-8)$ THz (d). (e) Black: shift-current contribution generated by pulse B alone. Red: corresponding nonlinear signal at $\tau = -0.7$ ps. (f) Symbols: Amplitudes of the Fourier transforms of $E_B(t)$ (black diamonds) and of $E_B(t) + E_{NL}(t,\tau)$ (cyan dots and magenta triangles) for two delay times [see dashed lines in (c)]. Solid lines: Gaussian fits to the data.

below 20 THz requires an even number of interactions with the electric field of pulse A and B [25], i.e., at least four interactions for the 2D experiment with two near-infrared pulses. The second-order interaction with the first pulse prepares the sample for another second-order interaction with the second pulse and, thus, the total nonlinear signal E_{NL} shown in Figs. 2(a)–2(d) is at least of fourth order in the near-infrared electric field. The $\chi^{(4)}$ signals in Fig. 2(b) are due to SC, TO, and hh ↔ lh emissions generated with A-B or B-A pulse sequences. The signal components discussed in the following are marked by arrows.

The SC signals originate from the nonlinear saturation of interband absorption. The first pulse excites an electron-hole plasma, which shifts the onset of interband absorption to higher frequencies via Pauli blocking of valence and conduction band states. As a consequence, the second near-infrared pulse displays a weaker interaction with the excited sample and, thus, induces THz emission with an electric field amplitude smaller than for interaction with an unpumped sample. In Fig. 2(e), the SC signal generated with pulse B alone (black curve) is shown as a function of real time t, together with the Fourier back transform of the 2D THz signal at $(\nu_t,\nu_\tau) = (2,0)$ THz for a delay time $\tau = -0.7$ ps, where pulse A interacts with the sample first and saturates the interband absorption. This nonlinear signal $E_{NL}(t,-0.7\text{ ps})$ shows a phase opposite to the single-pulse SC emission, a clear signature of nonlinear saturation.

The Raman processes generating the hh ↔ lh and TO phonon coherences are resonantly enhanced by the interband transition dipole at the GaAs band gap. Upon excitation of an electron-hole plasma, the blueshift of the absorption edge leads to a reduction of resonance enhancement and a concomitant decrease of the coherent amplitudes. This mechanism generates the nonlinear hh ↔ lh signals at $\nu_t = 12$ THz [Fig. 2(b)]. As the recombination time of the photogenerated electron-hole plasma is much longer than the time range of the 2D experiments, the nonlinear response caused by interband absorption saturation persists for picosecond delay times τ [cf. Fig. 2(a), [26]].

We now focus on the nonlinear TO phonon emission 2D signals represented by the peaks at $(\nu_t,\nu_\tau) = (8,0)$ and $(8,-8)$ THz. Their Fourier back-transforms display the nonlinear TO phonon emission induced by pulse B [Fig. 2(c)] and by pulse A [Fig. 2(d)]. In Fig. 2(d), the signal at negative delay times (pulse A interacts first) is due to the reduced Raman excitation efficiency by pulse B in the excited compared to an unexcited sample. At positive delay times, pulse B interacts first and generates a phonon coherence, which is perturbed by interaction with the second pulse A. The perturbation of the TO phonon free induction decay by pulse A is illustrated in Fig. 3, which shows the quantity $E^{TO}(t) = E^{TO}_{NL}(t,\tau) + E^{TO}_B(t)$, i.e., the sum of the 2D signal along t for two positive delay times τ and the TO phonon field emitted after interaction with pulse B only. The overall decay of the coherent phonon emission on a timescale of several picoseconds is caused by decoherence processes. Most interesting is the increase of the TO emission frequency after interaction with pulse A. Numerical fits of the high-precision time-domain data reveal a frequency upshift on the order of 100 GHz, i.e., 1% of the initial TO emission frequency. The Fourier spectra $|E_{TO}(\nu_t)|$ plotted in Fig. 2(f) exhibit the TO frequency upshift for $\tau > 0$ (dots) due to the stronger near-infrared pulse A and for $\tau < 0$ (triangles) due to the weaker pulse B. In the latter case, the upshift is smaller. It is

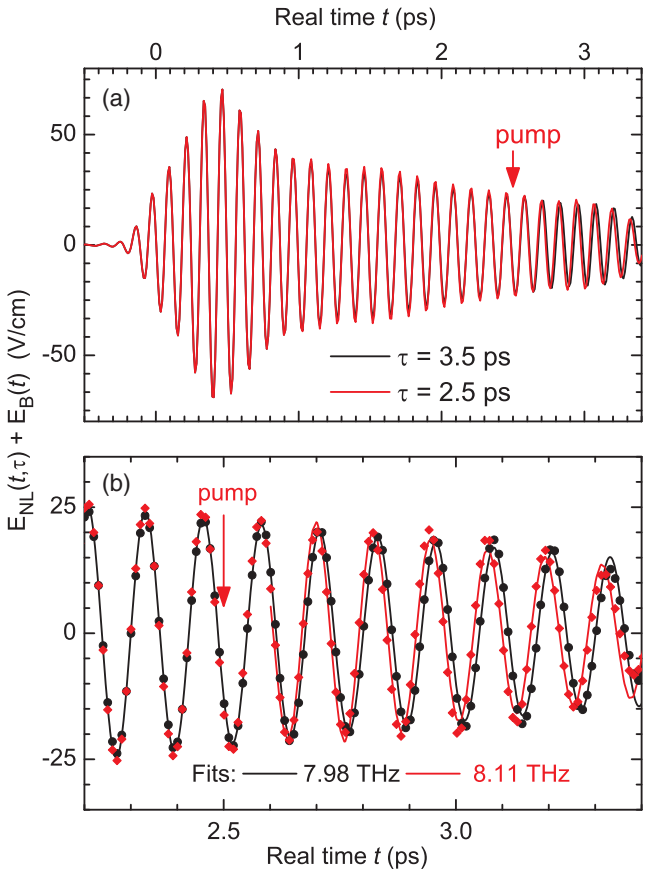

FIG. 3. (a) Measured THz transients $E_B^{\mathrm{TO}}(t) + E_{\mathrm{NL}}^{\mathrm{TO}}(t,\tau)$ emitted by TO phonons for two values of τ. In both cases the phonon coherence is induced by pulse B at $t = 0$. For the black curve ($\tau = 3.5$ ps) the pump pulse A arrives after the end of the time window shown. For the red curve ($\tau = 2.5$ ps) the pump pulse A (arrow) changes the THz emission frequency for later times. (b) Same experimental data in a stretched time window ($t = 2.2$ to 3.4 ps). Black solid line: fit of an exponentially decaying sine wave to the data for $\tau = 3.5$ ps (black dots). The data for $\tau = 2.5$ ps (red diamonds) lie on the black curve before the pump pulse, but afterwards their frequency is upshifted (red solid line) by $\Delta\nu_{\mathrm{TO}} \approx 100$ GHz.

important to note that the 2D technique applied here provides both the original and the slightly upshifted TO phonon frequency with high precision in a single measurement, a major advantage compared to much less sensitive pump-probe schemes with a single near-infrared excitation pulse.

There are two physical mechanisms that affect the TO phonon frequency observed in the THz emission from the excited GaAs crystal. First, interband excitation of carriers is connected with a local change of electronic charge density in the unit cell [Figs. 1(a)–1(c)]. This redistribution of charge affects the chemical bond strengths and modifies the vibrational potential of the TO phonons [28,29]. Upon interband excitation, charge is transferred from the covalent bonds between Ga and As atoms onto the Ga atoms, i.e., the bonds get weaker. The bond softening is a local effect and should result in a smaller force constant of the TO phonons and, thus, a redshift of the TO phonon frequency, in contrast to the experimental results. Apart from the wrong sign, the absolute values are way too low. When 2×10^{-4} electrons per unit cell are excited, one estimates a frequency shift of 80 MHz [29], 1000 times less than what is observed. A theoretical calculation of vibrational potentials in the excited GaAs sample is highly demanding and beyond the scope of the present experimental study.

Second, the photogenerated shift current is the source of a transient polarization, which modifies the long-range electric field in the sample and, thus, the frequency-dependent dielectric function. The change of the dielectric function shifts the observed TO phonon resonance and, thus, the frequency of the related THz emission. We assign the observed upshift of the TO phonon frequency, which is observed here for the first time, to this mechanism. This conclusion is supported by the theoretical estimate presented next.

The expected TO-phonon frequency upshift can be calculated with the help of the theoretical concepts of Refs. [6,7,10,11] and the experimental data of Ref. [14]. Without the electron-hole plasma the phonon contribution (including the background dielectric constant ε_∞) to the dielectric function is given by

$$\varepsilon_p(\nu) = \varepsilon_\infty + \frac{(\varepsilon_{\mathrm{st}} - \varepsilon_\infty)\nu_{\mathrm{TO}}^2}{\nu_{\mathrm{TO}}^2 - \nu^2 - i\nu\gamma}. \tag{1}$$

To account for the impact of the photogenerated shift current, one needs to consider the related changes of polarization and dielectric function. Such issues have been analyzed in detail in Refs. [10,11], where the related modification of the dielectric function has been calculated. The modified dielectric function is given by

$$\frac{\varepsilon(\nu) - 1}{\varepsilon(\nu) + 2} = \frac{\varepsilon_p(\nu) - 1}{\varepsilon_p(\nu) + 2} + \frac{\varepsilon_e(\nu) - 1}{\varepsilon_e(\nu) + 2}, \tag{2}$$

$$\text{with} \quad \varepsilon_e(\nu) = 1 - \frac{N_{\mathrm{eh}} e^2}{\varepsilon_0 m_0 4\pi^2 \nu^2}. \tag{3}$$

Here $\varepsilon_{\mathrm{st}}$ is the static dielectric constant, ν_{TO} the TO phonon frequency, γ the phonon damping, N_{eh} the volume density of the electron-hole plasma, and m_0 the free-electron mass. Equation (3) contains the free-electron mass and not the effective mass because the electron motion leading to the shift current [cf. Figs. 1(b) and 1(c)] occurs over a small distance within the unit cell.

From Eq. (2), one derives an almost linear frequency upshift of the TO phonon resonance as a function of electron-hole density. For $N_{\mathrm{eh}} = 10^{17}$ cm^{-3}, the frequency shift has a value of $\Delta\nu_{\mathrm{TO}} = 100$ GHz [30], in good agreement with our experimental observation. The agreement

with experiment supports the conclusion that changes of TO phonon frequency due to a modification of the vibrational potential are substantially smaller.

In conclusion, two-dimensional nonlinear spectroscopy provides the first direct evidence for the impact of electronic shift currents on the TO phonon resonance in the prototype semiconductor GaAs. Highly accurate time-domain data reveal a frequency upshift of the TO phonon emission by 100 GHz, which is due to the change of the dielectric function originating from a transient interband shift current. Our results show that the TO phonon emission frequency of GaAs is a most sensitive probe of subtle changes in the electronic charge distribution and Coulomb correlations among carriers. The observed behavior is expected to occur in a wide range of semiconductors and insulators, in particular in materials with a high polarity of the crystal lattice such as ferroelectrics and polar quantum materials.

We acknowledge financial support by the Deutsche Forschungsgemeinschaft: WO 558/14-1 and RE 806/9-1.

*woerner@mbi-berlin.de

[1] M. Born and K. Huang, *Dynamical Theory of Crystal Lattices* (Oxford University Press, London, 1954).

[2] W. Cochran, Crystal stability and the theory of ferroelectricity, Adv. Phys. **9**, 387 (1960).

[3] G. Folpini, K. Reimann, M. Woerner, T. Elsaesser, J. Hoja, and A. Tkatchenko, Strong Local-Field Enhancement of the Nonlinear Soft-Mode Response in a Molecular Crystal, Phys. Rev. Lett. **119**, 097404 (2017).

[4] I. Katayama, H. Aoki, J. Takeda, H. Shimosato, M. Ashida, R. Kinjo, I. Kawayama, M. Tonouchi, M. Nagai, and K. Tanaka, Ferroelectric Soft Mode in a $SrTiO_3$ Thin Film Impulsively Driven to the Anharmonic Regime Using Intense Picosecond Terahertz Pulses, Phys. Rev. Lett. **108**, 097401 (2012).

[5] C. Hauf, A.-A. H. Salvador, M. Holtz, M. Woerner, and T. Elsaesser, Soft-mode driven polarity reversal in ferroelectrics mapped by ultrafast x-ray diffraction, Struct. Dyn. **5**, 024501 (2018).

[6] J. H. Hannay, The Clausius-Mossotti equation: An alternative derivation, Eur. J. Phys. **4**, 141 (1983).

[7] M. Bucher, Revaluation of the local field, J. Phys. Chem. Solids **51**, 1241 (1990).

[8] A. M. Reilly and A. Tkatchenko, Role of Dispersion Interactions in the Polymorphism and Entropic Stabilization of the Aspirin Crystal, Phys. Rev. Lett. **113**, 055701 (2014).

[9] C. Hauf, A.-A. H. Salvador, M. Holtz, M. Woerner, and T. Elsaesser, Phonon driven charge dynamics in polycrystalline acetylsalicylic acid mapped by ultrafast x-ray diffraction, Struct. Dyn. **6**, 014503 (2019).

[10] S. L. Adler, Quantum theory of the dielectric constant in real solids, Phys. Rev. **126**, 413 (1962).

[11] N. Wiser, Dielectric constant with local field effects included, Phys. Rev. **129**, 62 (1963).

[12] G. S. Spencer, A. C. Ho, J. Menéndez, R. Droopad, H. Fathollahnejad, and G. N. Maracas, Lattice-constant dependence of the dynamical effective charge in AlAs and GaAs, Phys. Rev. B **50**, 14125 (1994).

[13] M. Holtz, M. Seon, O. Brafman, R. Manor, and D. Fekete, Pressure dependence of the optic phonon energies in $Al_xGa_{1-x}As$, Phys. Rev. B **54**, 8714 (1996).

[14] D. J. Lockwood, G. Yu, and N. L. Rowell, Optical phonon frequencies and damping in AlAs, GaP, GaAs, InP, InAs and InSb studied by oblique incidence infrared spectroscopy, Solid State Commun. **136**, 404 (2005).

[15] B. Tell and R. J. Martin, Raman scattering by coupled optical-phonon-plasmon modes in GaAs, Phys. Rev. **167**, 381 (1968).

[16] C. G. Olson and D. W. Lynch, Longitudinal-optical-phonon-plasmon coupling in GaAs, Phys. Rev. **177**, 1231 (1969).

[17] A. M. Glass, D. von der Linde, and T. J. Negran, High-voltage bulk photovoltaic effect and the photorefractive process in $LiNbO_3$, Appl. Phys. Lett. **25**, 233 (1974).

[18] V. L. Alperovich, V. I. Belinicher, V. N. Novikov, and A. S. Terekhov, Photogalvanic effects investigation in gallium arsenide, Ferroelectrics **45**, 1 (1982).

[19] R. von Baltz and W. Kraut, Theory of the bulk photovoltaic effect in pure crystals, Phys. Rev. B **23**, 5590 (1981).

[20] F. Nastos and J. E. Sipe, Optical rectification and shift currents in GaAs and GaP response: Below and above the band gap, Phys. Rev. B **74**, 035201 (2006).

[21] A. Ghalgaoui, K. Reimann, M. Woerner, T. Elsaesser, C. Flytzanis, and K. Biermann, Resonant Second-Order Nonlinear Terahertz Response of Gallium Arsenide, Phys. Rev. Lett. **121**, 266602 (2018).

[22] W. Kuehn, K. Reimann, M. Woerner, and T. Elsaesser, Phase-resolved two-dimensional spectroscopy based on collinear n-wave mixing in the ultrafast time domain, J. Chem. Phys. **130**, 164503 (2009).

[23] T. Elsaesser, K. Reimann, and M. Woerner, *Concepts and Applications of Nonlinear Terahertz Spectroscopy* (Morgan & Claypool Publishers, San Rafael, CA, USA, 2019).

[24] The frequency range is limited by the EO sampling detection bandwidth.

[25] In contrast, an odd number of interactions always generates nonlinear signals with detection frequencies of at least 350 THz, which are not considered here.

[26] Both the SC and the hh $\leftrightarrow$ lh signals occur only in the range of sequential pump-probe interactions, while a perturbed free-induction decay is absent [27].

[27] M. Chachisvilis, H. Fidder, and V. Sundström, Electronic coherence in pseudo two-colour pump-probe spectroscopy, Chem. Phys. Lett. **234**, 141 (1995).

[28] J. C. Phillips, Ionicity of the chemical bond in crystals, Rev. Mod. Phys. **42**, 317 (1970).

[29] S. Steiger, M. Salmani-Jelodar, D. Areshkin, A. Paul, T. Kubis, M. Povolotskyi, H.-H. Park, and G. Klimeck, Enhanced valence force field model for the lattice properties of gallium arsenide, Phys. Rev. B **84**, 155204 (2011).

[30] The values given here are valid for perfectly localized electrons, which is a good approximation for the case here. For partially localized electrons [31], the phonon shift will be smaller.

[31] R. F. Guertin and F. Stern, Effective fields in cubic lattices with extended charges, Phys. Rev. **134**, A427 (1964).